A medium-scale traveling ionospheric disturbance observed from the ground and from space

K. F. Dymond,[1] C. Watts,[2,3] C. Coker,[1] S. A. Budzien,[1] P. A. Bernhardt,[4] N. Kassim,[5] T. J. Lazio,[5,6] K. Weiler,[5] P. C. Crane,[5,7] P. S. Ray,[1] A. Cohen,[5,8] T. Clarke,[5] L. J. Rickard,[9] G. B. Taylor,[9] F. Schinzel,[9,10] Y. Pihlstrom,[9] M. Kuniyoshi,[9,10] S. Close,[11,12] P. Colestock,[12] S. Myers,[13] and A. Datta[13,14]

Received 30 September 2010; revised 31 May 2011; accepted 14 June 2011; published 30 September 2011.

[1] We report ultraviolet optical observations from space of a Medium-Scale Traveling Ionospheric Disturbance (MSTID) made during the Combined Radio Interferometry and COSMIC Experiment in Tomography Campaign (CRICKET) held on September 15, 2007 at ~8:30 UT. The experiment used a Constellation Observing System for Meteorology, Ionosphere, and Climate (COSMIC also known as FORMOSAT-3) satellite in conjunction with the Very Large Array (VLA) radio telescope, located near Socorro, NM, to study the ionosphere from the global scale down to the regional scale while the TIDs propagated through it. The COSMIC/FORMOSAT-3 satellite measured the *F* region electron density both horizontally and with altitude while the VLA measured the directions and speeds of the TIDs. These observations provide new information on this poorly understood class of TID and demonstrate the possibility of studying MSTIDs using space-based optical instruments.

Citation: Dymond, K. F., et al. (2011), A medium-scale traveling ionospheric disturbance observed from the ground and from space, *Radio Sci.*, *46*, RS5010, doi:10.1029/2010RS004535.

1. Introduction

[2] Radio astronomy measurements can be strongly impacted by atmospheric effects that below about 1.4 GHz are typically dominated by the Earth's ionosphere. Variations in total electron content (TEC) over different antennas commonly disrupt the phase coherence of large radio interferometers like the Very Large Array (VLA - maximum antenna separation ~35 km). Consequently, the data must be corrected [*Kassim et al.*, 2007] to recover the cosmic source visibility (amplitude and phase) to permit high angular resolution imaging and accurate radio flux density measurements of cosmic background emitters. At the same time, these corrections can provide a powerful probe about the structure of the regional ionosphere between the interferometer and the distant radio sources. Previous ionospheric studies using the VLA and other radio interferometers have indicated the presence of TIDs of various scales and smaller scale structures due to the plasmasphere [*Mercier*, 1986; *Jacobson and Erickson*, 1992a, 1992b, 1993; *Kassim*, 2007]. The next generation large, low frequency radio interferometers (e.g., the LWA: http://lwa.unm.edu and LOFAR: http://www.lofar.org) will be much larger (>100 km) and more sensitive (e.g., MWA: http://www.haystack.mit.edu/ast/arrays/mwa/index.html) than the VLA and will provide exciting opportunities for ionospheric research on the regional level if the ionospheric effects can be effectively modeled and understood.

[3] Previous Medium-Scale TID (MSTID) studies in the southwestern United States using the VLA, a satellite-radio beacon interferometer, and the GPS network have shown that nighttime MSTID propagation is typically toward the southwest at speeds between 50 to >300 m s^{-1}, with wavelengths of 200–250 km, and periods of 10s of minutes [*Jacobson and Erickson*, 1992a, 1992b; *Jacobson et al.*, 1995; *Afraimovich et al.*, 2003; *Kotake et al.*, 2007; *Tsugawa et al.*, 2007]. The lengths of the wavefronts of MSTIDs were found to be very

[1]Space Science Division, Naval Research Laboratory, Washington, D. C., USA.
[2]Department of Electrical and Computer Engineering, University of New Mexico, Albuquerque, New Mexico, USA.
[3]Diagnostics Division, ITER, St Paul Lez Durance, France.
[4]Plasma Physics Division, Naval Research Laboratory, Washington, D. C., USA.
[5]Remote Sensing Division, Naval Research Laboratory, Washington, D. C., USA.
[6]Jet Propulsion Laboratory, Pasadena, California, USA.
[7]Socorro, New Mexico, USA.
[8]Applied Physics Laboratory, Johns Hopkins University, Laurel, Maryland, USA.
[9]Department of Physics and Astronomy, University of New Mexico, Albuquerque, New Mexico, USA.
[10]Max-Planck-Institut für Radioastronomie, Bonn, Germany.
[11]Department of Aeronautics and Astronautics, Stanford University, Stanford, California, USA.
[12]Los Alamos National Laboratory, Los Alamos, New Mexico, USA.
[13]National Radio Astronomy Observatory, Socorro, New Mexico, USA.
[14]Center for Astrophysics and Space Astronomy, University of Colorado, Boulder, Colorado, USA.

0048-6604/11/2010RS004535

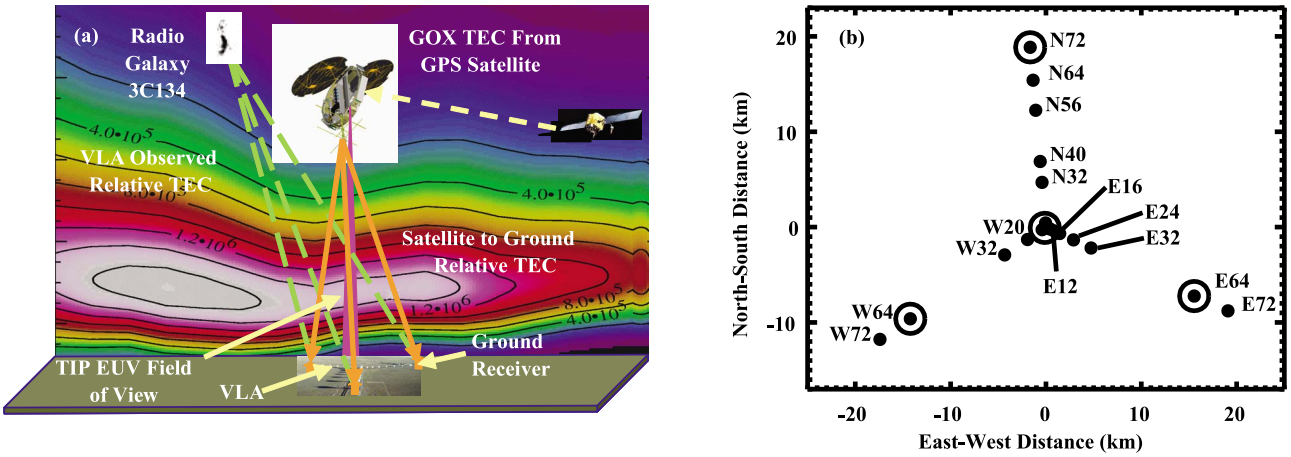

Figure 1. CRICKET Concept. (a) The experiment concept. (b) The VLA in the A-configuration. The antennas used in the campaign are indicated, with circles indicating the antennas with co-located TBB receivers. The antennas nearest the center of the array overlap in this figure and hence are not visible.

long ~2000 km, by *Tsugawa et al.* [2007], using the GPS network over the United States. Using a dense array of GPS receivers in the southwestern U.S., *Afraimovich et al.* [2003] identified a new class of TID, the Traveling Wave Packet TID (TWPTID), which appear as wave packets with sinusoidal modulation and Gaussian envelopes. MSTIDs are known to be generated by gravity waves induced by auroral activity, by wind flow over mountains, jet stream generated turbulence, and by other sources [*Schunk and Nagy*, 2000].

[4] The six-satellite Constellation Observing System for Meteorology, Ionosphere, and Climate (COSMIC/FOMOSAT-3, CF3 in this work) satellite constellation was launched on April 15, 2006 as a joint venture between the United States and the Republic of China (Taiwan) [*Anthes et al.*, 2008]. Each CF3 satellite carries three instruments to study the Earth's ionosphere: the GPS Occultation Experiment (GOX), the Tiny Ionospheric Photometer (TIP), and the Tri-Band Beacon (TBB). The CF3 satellites are a powerful means of studying and specifying the nighttime ionosphere from the global scale down to the regional scale using a combination of the measurements.

[5] The Combined Radio Interferometry and COSMIC Experiment in Tomography (CRICKET) was proposed to perform ionospheric measurements over the VLA and to tie these measurements to the global and regional ionospheric structure determined by tomographic inversion of the CF3 measurements [*Dymond et al.*, 2000, 2009a; *Dymond and Thomas*, 2001]. The goal of the CRICKET campaign was to use the VLA to explore ionospheric phenomena that would affect operation of the Long Wavelength Array (LWA: http://lwa.unm.edu) radio-interferometer under construction in New Mexico. Epoch 1 of the campaign occurred on September 15, 2007 from 08:00–09:20 UT; the 10.7 cm solar flux was 68.5×10^{-22} w m^{-2} Hz^{-1} and the a_p was 3 nT, indicating geomagnetically quiet conditions typical to solar minimum. Preliminary analyses of the data in this work were presented by *Dymond et al.* [2008] and *Watts et al.* [2008]. Figure 1a shows the concept for the measurements while Figure 1b shows the VLA configuration and the locations of the TBB receivers. Although the TBB beacon data were gathered, due to a campaign slip the lines-of-sight between the TBB receivers and the CF3 satellite were partially blocked by the VLA antennas rendering the data useless and so this work will concentrate in the GOX, TIP, and VLA measurements. During the campaign MSTIDs were observed with VLA and TIP while the GOX measured the background ionosphere in which the TIDs propagated. Using these measurements, we were able to infer the TEC amplitudes, speeds, wavelengths, and periods of the TIDs and confirm the optical observation of a MSTID from space.

2. Measurements and Analysis

2.1. GOX GPS Occultation

[6] Figure 2a shows the electron density profiles of three widely separated occultations (indicated by the GPS satellite PRN number) produced by Abel inversion of the slant TEC measured by the GOX on CF3 satellite #4; these profiles were downloaded from the COSMIC Data Acquisition and Analysis Center web site (COSMIC Data Acquisition and Analysis Center (CDAAC), September 2007, http://cosmic-io.cosmic.ucar.edu/cdaac/login/cosmic/, accessed 6 June 2008). The shapes of the three profiles are similar and only small density scaling and shifts in altitude are required to get all three profiles to lie on top of each other thus indicating that the background ionosphere was very smooth with low height and density gradients. The profile closest to the VLA was from GPS satellite #19 (see Figure 2b). The ionospheric parameters from this profile are: *F* region peak height (hmF2) ~ 290 km, *F* region peak density (nmF2) ~ 1.5×10^5 cm^{-3}, and vertical total electron content (vTEC) ~2.7 TECU (1 TECU = 10^{12} electrons-cm^{-2}). The vertical TEC was calculated by vertically integrating the electron density from the profile and converting to TECU. The CF3 satellite passed over western Oklahoma into central Texas during the TIP observations as shown in Figure 2b.

2.2. VLA Measurements

[7] During the campaign, the VLA observed at 73.8 MHz in the A-configuration (largest antenna separation ~35 km, Figure 1b), with 20 antennas in operation. The VLA observed the ionosphere which was back illuminated by

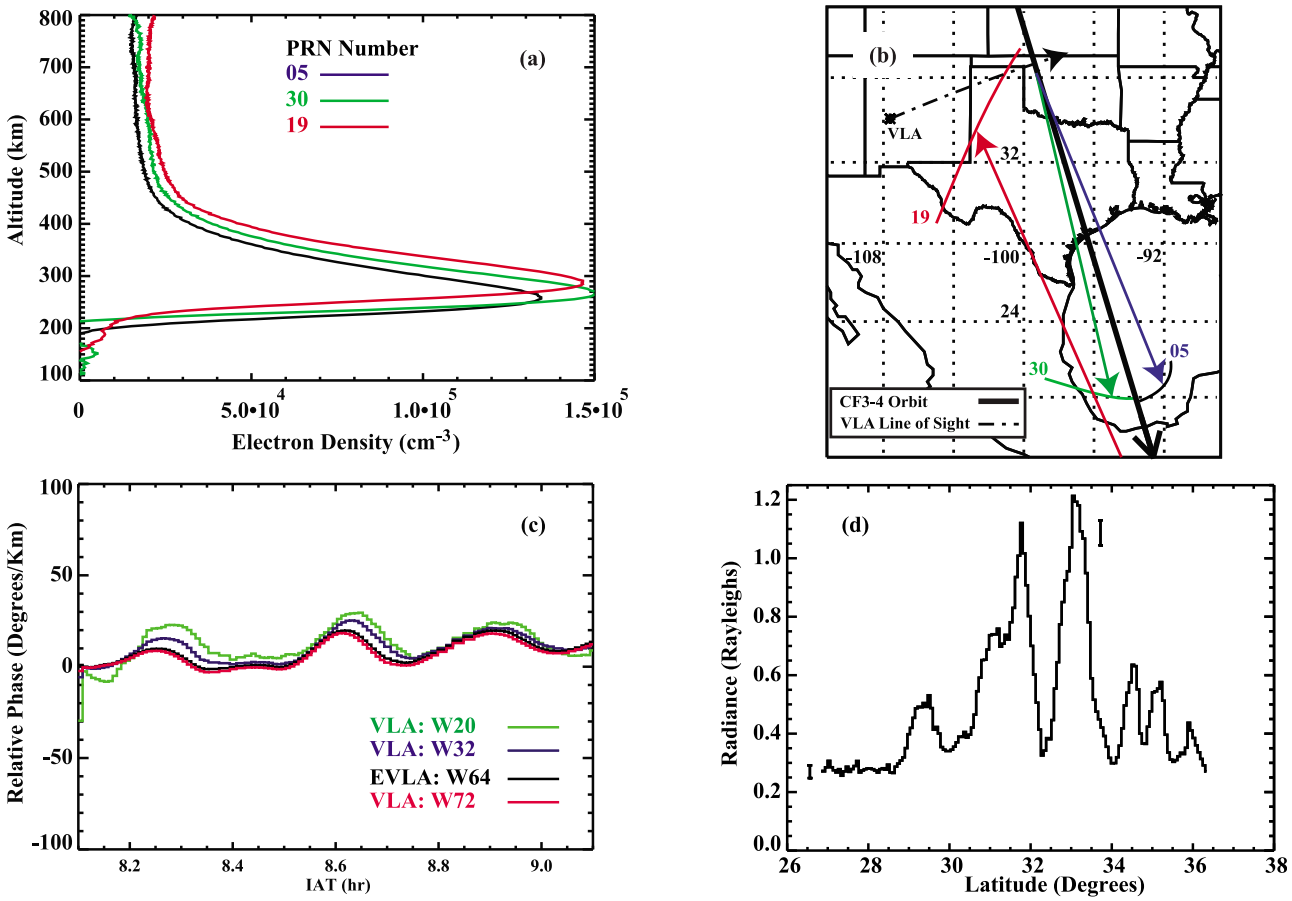

Figure 2. Campaign Measurements. (a) The electron density profiles from three occultations in the American sector. (b) The satellite orbit and the tangent point trajectories for the occultations with the VLA location indicated by the "*." The occultation lines-of-sight are indicated by the colored arrows. The CF3 satellite moved from north to south as indicated by the large arrow on the orbit. (c) The baseline reduced phases along the Southwestern arm of the VLA. (d) The observed TIP radiances with representative ±2-σ error bars to indicate the precision of the measurements.

bright radio source 3C134, at right ascension $05^h\ 01^m\ 17.23^s$ and declination $+38°\ 2^m\ 6.1^s$. As astrophysical emitters are effectively at infinite distance, the lines-of-sight from individual antennas probe the ionosphere with spatial sampling determined by the projected separation of antennas in the direction of the source. Because the absolute phase of the radio source is not a known quantity, the VLA measured the ionospherically induced phase relative to the antenna nearest the center of the array (W4) at 3 min cadence from 08:00–09:20 UT. The phase measurements are stable to ~1° corresponding to ~0.0015 TECU at 73.8 MHz. As the bright radio source dominated the radio flux, the phase differences observed by the VLA antennas were caused primarily by ionospheric plasma lying between the radio source and the VLA antennas. Figure 2c shows the observed phases along the Southwestern arm divided by the baseline length (baseline reduced phases). In ionospheres with linear TEC gradients, the ionospherically induced phase differential is proportional to the baseline length. Wave structures are clearly seen in this plot of phase differences along the Southwest arm. The phase progressions along the North and Southeast arms (not shown) show similar phase structures.

[8] Following *Jacobson and Erickson* [1992a], the relative VLA antenna phases between 8.2 and 9.0 UT (~48 min duration) were fit to extract plane wave TID solutions. In an attempt to reduce the effects of phase contamination by weaker secondary radio sources in the radio telescope's fields-of-view (~12° at 74 MHz), the phases were averaged along all of the interferometer baselines, using the method suggested by *Jacobson and Erickson* [1992a]. The Jacobson and Erickson method takes advantage of phase closure between groups of antennas to average out the secondary source contributions. Phase closure states that the sum of the phase differences when a closed loop is traversed among antenna groups is 0°, modulo 360°. The phases are averaged using the formula taken from the work of *Jacobson and Erickson* [1992a], *viz*:

$$\langle \Phi \rangle_{mn} \equiv \frac{1}{N-1} \left\{ \Phi_{mn} + \sum_{\substack{j=1,N \\ j \neq m,n}}^{N} \left[\Phi_{jn} - \Phi_{jm} \right] \right\}$$

where Φ_{mn} indicates the measured phase difference (including the ionospherically induced phase and the secondary

Table 1. TID Parameters Derived From VLA Measurements[a]

P (minutes)	A (TECU)	λ (km)	Az. (°)	v (m/s)	Λ (km)
47.7 ± 15.9	0.05 ± 0.005	284.8 ± 39.2	238 ± 8.4	100 ± 33	1266 ± 174
23.8 ± 6.0	0.28 ± 0.03	215.0 ± 2.1	232 ± 0.6	199 ± 25	875 ± 10
15.9 ± 1.3	0.19 ± 0.02	158.1 ± 1.0	242 ± 0.7	166 ± 14	1010 ± 9
13.6 ± 1.0	0.07 ± 0.01	78.7 ± 1.0	223 ± 1.4	96 ± 7	168 ± 2
11.9 ± 0.8	0.14 ± 0.02	178.6 ± 3.4	121 ± 1.0	250 ± 17	233 ± 5
10.6 ± 0.6	0.14 ± 0.02	196.1 ± 2.4	159 ± 1.5	308 ± 17	196 ± 3

[a]P, wave period; A, wave amplitude; λ, wavelength, Az., wave propagation azimuth measured clockwise North through East; v, wave speed; and Λ, TID wavelength projected onto CF3–4 orbit plane.

source phase) between antennas m and n and the $\langle\ \rangle$ indicates the average. Jacobson and Erickson show that the secondary source contributions to the phase tend to average out leaving only the ionospheric contribution. After phase averaging, the phase progressions were Fourier transformed in the time domain. Then, at each temporal frequency f, the antenna phases were fit with a plane wave model and at each frequency the wave amplitude, wavelength, direction of travel (azimuth) and phase speed were retrieved. So that confidence limits could be established for the detection of a given wave, the error bars for the Fourier transforms were calculated using the known phase measurement errors (~1.5°) and standard propagation of error formulae [*Bevington*, 1969]. Thus, the error bars on the phase amplitude could be accurately determined and used in subsequent chi-square fitting to determine the characteristics of the TIDs. The spatial characteristics were determined by fitting the following plane wave model:

$$\hat{\Phi}^f = \hat{\Phi}^f_m \cos\left(\Omega_f(t - t_0) - \vec{k}_f \circ \vec{x} + \varphi_f\right) \quad (1)$$

where Φ^f_m is the amplitude of the antenna phase at temporal frequency f, Ω is 2π divided by the wave period in minutes, t is the observation time in minutes, t_0 is the start time of the observation, $\vec{k}_f$ is the wave number (2π divided by the wavelength in km – a vector quantity as indicated by the arrow), $\vec{x}$ is the location of the VLA antenna (a vector quantity), and φ_f is the phase of the wave at $t = t_0$. The "^" indicates that the Fourier-transformed relative phase at the antenna is used in the fit. As shown in Table 1, several plane waves traveling at a variety of speeds and in a variety of directions were detected.

2.3. TIP Measurements

[9] The TIP measures the UV radiance at 135.6 nm (Figure 2d) which is primarily created by radiative recombination of F region O^+ ions and electrons to produce atomic oxygen in an excited state that decays with the emission of the photon. A secondary emission source is electron attachment to form O^-, which then neutralizes with O^+ resulting in an excited O atom that radiatively decays. The 135.6 nm emission is essentially optically thin so that the radiance is proportional to the integral over altitude of the volume emission rate, which is proportional to the product of the O^+ and electron densities. The photochemical processes responsible for the emission are summarized by *Meléndez-Alvira et al.* [1999] and *Tinsley and Bittencourt* [1975]; the reaction rates are those from the work of *Meléndez-Alvira et al.* [1999]. In the nightglow observations mode, the sensitivity of the TIP instruments ranges from ~500–1200 ct-s^{-1}Rayleigh^{-1} [*Budzien et al.*, 2009; *Dymond et al.*, 2009a] so that the statistical uncertainties in the measurements are small, ~3%. During operations aboard the CF-3 satellites, the TIP instruments change modes to protect them from the bright daytime airglow and to enable nighttime and auroral zone measurements [*Budzien et al.*, 2009]. During the CRICKET observations, the TIP instrument experienced a mode change immediately prior to the observations reported in this work. The instrument changed from pinhole or auroral observation mode to nightglow observation mode, where the instrument is more sensitive. The measurements reported in this work occurred just after the CF3–4 satellite crossed the line-of-sight of the VLA so the TIP and VLA measurements are nearly, but not perfectly, coincident.

[10] We fit the TIP count rates using a model of the 135.6 nm emission which included both sources discussed above. The NRLMSISE-00 [*Picone et al.*, 2002] thermospheric density model was used to estimate the O density needed to calculate the neutralization rate. The fitting procedure assumed that the vertical electron and, via charge neutrality, ion density distri-

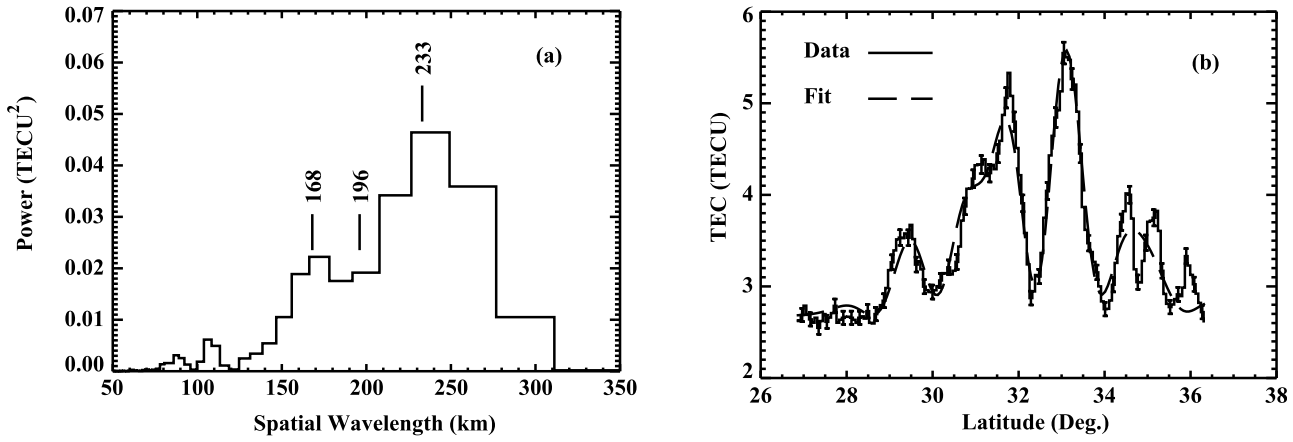

Figure 3. TIP Observations. (a) The Fourier transform of the vertical TEC inferred from the TIP observations with the projected TID wavelengths indicated. (b) The inferred TEC distribution along the orbit plane derived from the TIP and GOX data; representative ±2-σ error bars are shown to indicate the uncertainty in the inferred vertical TEC. The dashed line shows the Gaussian modulated TID model fit.

Table 2. TID Parameters Derived From TIP Measurements[a]

VLA Proj. Λ (km)	Λ (km)	Peak Amplitude (TECU)	Amplitude at VLA LOS (TECU)
233	239 ± 1	2.1 ± 0.27	0.14 ± 0.018
196	188 ± 5	0.7 ± 0.10	0.05 ± 0.007
168	162 ± 2	1.0 ± 0.16	0.07 ± 0.011

[a]VLA Proj. Λ, TID wavelength projected onto COSMIC orbit plane; Λ, TID wavelength from TIP observations.

bution, was that measured by the GOX in the GPS occultation nearest to the VLA (PRN #19). For each pixel of the TIP measurements, the peak electron density, n_mF2, was varied to scale the entire electron density profile to match the measurements. The vTEC (vertical TEC) inferred from the TIP data using the fitting procedure is shown in Figure 3b. The vTEC data show a variation that is similar to a Gaussian with a sinusoidal modulation. However, upon closer inspection, the TIP vTEC data show evidence of several wavelengths, which is consistent with some of the wavelengths from our VLA observations when projected to the CF3 orbit plane.

[11] *Afraimovich et al.* [2003] identified a new class of TID, the Traveling Wave Packet TID (TWPTID), using a dense array of GPS receivers in the southwestern U.S.. TWPTIDs appear as quasiperiodic wave packets with Gaussian envelopes of width ~1 h. and sinusoidal modulation at periods of 10–20 min., which suggests they may be associated with acoustic-gravity waves. This type of TID is rare, appearing on 0.1–0.4% of the GPS-receiver links in the Afraimovich et al. study. The VLA analysis indicated the presence of MSTIDs, while the TIP data showed what appeared to be a Gaussian packet shape with wavelike modulation. A spatial Fourier transform of the TIP data shows the presence of three dominant waves (Figure 3a). When taken together, these observations are similar to a TWPTID. The TIP measurements were fit using an ad hoc superposition of a set of three sine waves modulated by a single Gaussian envelope using a functional form similar to that used by *Afraimovich et al.* [2003], *viz.*:

$$TEC = \sum_i \frac{TEC_i}{2} \exp\left(-\frac{(x-x_p)^2}{2\sigma^2}\right)(1+\sin(\Omega_i(t-t_0) - k_i x + \varphi_i)) + TEC_B \quad (2)$$

where TEC_i is the TEC at the peak of the Gaussian for each wave, x_p is the position of the peak along the orbit plane, x is the distance along the orbit plane, σ is the width of the Gaussian, Ω_i is 2π divided by the wave period, k_i is 2π divided by the wavelength of the sine wave, φ_i is the phase of the wave at $x = 0$, and TEC_B is a constant TEC background. Because the total duration of the TIP measurements, $(t - t_0) = 1.5$ min., is much less than the periods of the waves observed by the VLA, the first term in the argument of the sine was fixed and captured in the phase. The results of the Gaussian TID fit are shown in Table 2 and the fit to the TIP data is shown as the dashed line Figure 3b; the agreement between the model and the data is very good.

3. Results and Discussion

[12] The TID fit to the TIP data included three waves and is in good agreement with the VLA wavelengths of the waves with periods shorter than ~14 min (Table 1). To compare the wavelengths of the waves from the TIP and VLA measurements, the waves observed by the VLA were projected onto the CF3 orbit plane, which was at an azimuth of 161°. The fit to the TIP data yielded wavelengths of 239 ± 1 km, 188 ± 5 km, and 162 ± 2 km, while the projected VLA wavelengths are 233 ± 5, 196 ± 3, and 168 ± 2 km. The wavelengths for the three waves are in excellent agreement. The wave speeds derived from the analysis are 250 ± 17, 308 ± 17, and 96 ± 7 m s^{-1} respectively, which when combined with the wave periods of 11.9 ± 6.3, 10.6 ± 3.5, and 13.6 ± 3.5 min., place these waves in the MSTID class. Adopting the two times the full width at half maximum of the Gaussian modulation of the TID as the total width of the packet, the packet is ~1078 ± 17 km in reasonable agreement with the *Afraimovich et al.* [2003] value of ~700 km, based on a typical TWPTID duration (~1 h) and speed of ~200 m s^{-1}. While it is unlikely the TID observed by the TIP is a TWPTID because it is best reproduced by a superposition of TIDs, it is interesting that the observed packet width agrees with typical TWPTIDs.

[13] The speeds, wavelengths, periods, and amplitudes of the TIDs seen by the VLA (Table 1) are consistent with previous observations of medium-scale traveling ionospheric disturbances (MSTIDs) [*Jacobson and Erickson*, 1992a, 1992b; *Jacobson et al.*, 1995; *Afraimovich et al.*, 2003; *Kotake et al.*, 2007; *Tsugawa et al.*, 2007]. Although the waves with 23.8, 11.9, and 10.6 min periods have speeds >200 m s^{-1} and are traveling faster than typical nighttime MSTIDs with speeds of ~100–150 m/s, they are still moving slower than the speed of sound in the thermosphere (~ 1 km s^{-1}) and are within the speed range associated with MSTIDs [*Hocke and Schlegel*, 1996]. The wavelengths inferred from the VLA analysis and the wave periods (in the tens of minutes range) suggest these TIDs are driven by acoustic-gravity waves. The amplitudes of the TIDs seen by the VLA are seen to be much lower than those seen near the peak of the MSTIDs observed by the TIP. However, when the amplitudes of the waves seen by the TIP are calculated at the intersection of the VLA's line-of-sight with the CF3 orbit plane (because the TIP and VLA measurement are not perfectly coincident), the TEC amplitudes for the waves with 239, 188, and 162 km wavelengths are 0.14, 0.05, and 0.07 TECU, and are in reasonable agreement with those observed by the VLA, 0.14, 0.14, and 0.07 TECU, at projected wavelengths of 233, 196, and 165 km.

[14] The two most intriguing aspects of the TIP MSTID observations (Figure 3) are that the modulation does not show both positive and negative TEC excursions about a fixed background, typical of most radio wave observations, and the magnitude of the TEC variations is comparable to the background of ~2.7 TECU. As shown in Table 2, the peak amplitudes of the three component waves are 2.1, 0.7, and 1.0 TECU, ~10 times larger than the TEC amplitudes of the MSTIDs observed by *Tsugawa et al.* [2007] and the most probable TWPTID amplitude seen by *Afraimovich et al.* [2003]; although the latter did observe TEC amplitudes > 1 TECU, more consistent with the TIP measurements. In addition to the TWPTIDs, non-periodic TIDs have been reported having only increases or decreases from the background TEC [*Francis*, 1975; *Titheridge*, 1971]. Note that because the VLA measures TEC relative to a reference

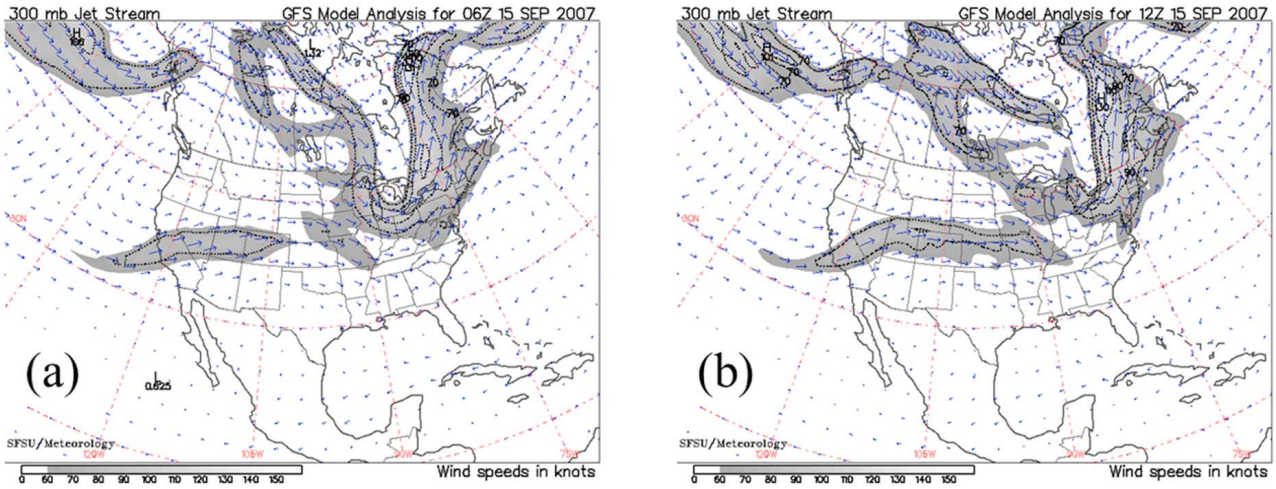

Figure 4. Maps of the Jet Stream over the United States on September 15, 2007 at (a) 6 UT and (b) 12 UT. The CRICKET observations occurred at ~8:30 UT.

antenna, which is akin to measuring the spatial derivative of the TEC, the VLA cannot determine if the TEC in an MSTID is only a positive or negative perturbation atop a background.

[15] We performed a quick survey to try to determine where and how the TIDs were generated. MSTIDs are known to be generated by gravity waves induced by auroral activity, wind flow over mountains, jet stream generated turbulence, and by other sources [*Schunk and Nagy*, 2000]. Auroral activity on Sept. 15, 2007 was low, so we have ruled out generation near the auroral zone as a likely origin. TIDs are frequently observed by the VLA. Some of these waves are likely to be generated locally by wind flow over the mountains of Western New Mexico. Table 1 shows that there are several waves traveling at azimuths from 121 to 243°. However, since the many of the waves are propagating southwesterly and the ionospheric pierce point (~290 km based on GOX measurements) of the VLA's field-of-view occurred far to the east of the Rocky Mountains, it is unlikely they were generated by mountain waves as this would require eastward or southeastward directions of propagation to be observed by the CF-3 satellite. Maps of the jet stream on September 15 (Figure 4) showed that it was changing rapidly over the central U.S. prior to and during our observations (North America Jet Stream Map Archive, California Regional Weather Server, San Francisco State University, September 2007, http://virga.sfsu.edu/pub/jetstream/jetstream/big/0709/, accessed 26 May 2011). At 6 UT on September 15, the southern-most extent of a "u-shaped" bend in the jet stream was located approximately northeastward of New Mexico and Central Texas. That the waves are moving either toward the southwest or the southeast lends credence to the conjecture that the acoustic-gravity waves driving the TIDs may have originated there. We note, however, that previous studies of MSTIDs in the U.S. found the climatology of the nighttime propagation direction tends to peak toward the Southwestern direction [*Tsugawa et al.*, 2007; *Jacobson and Erickson*, 1992b]. Additional work is needed to resolve whether the waves were generated by jet stream turbulence or whether they were generated as part of whatever mechanism is driving the MSTID climatology.

[16] Gravity waves and MSTIDs are likely to have complex three-dimensional structure including tilted wavefronts and vertical propagation of the gravity waves [*Schunk and Nagy*, 2000; *Hickey et al.*, 2010; *Hocke and Schlegel*, 1996]. While a more detailed analysis of the MSTID/gravity waves reported here would require the three-dimensional modeling and detailed accounting for the passage of the lines-of-sight through the structure, we opted for simpler analyses based upon previously demonstrated methods. The primary goal of this work was to demonstrate the feasibility of observing MSTIDs from space using optical sensors. The feasibility of using satellite-based UV sensors has been demonstrated using the analysis technique of *Jacobson and Erickson* [1992a] and a variation of the techniques described by *Dymond et al.* [2000] and *Dymond and Thomas* [2001].

4. Summary and Conclusions

[17] A medium-scale TID with sharing characteristics with the Traveling Wave Packet Traveling Ionospheric Disturbances seen by *Afraimovich et al.* [2003] and the non-periodic TIDs observed and reported by *Titheridge* [1971] was observed during the multi-instrument CRICKET campaign on September 15, 2007 at ~8:30 UT. The optical characteristics of the observed TID indicated a positive TEC modulation on top of the background TEC, in contrast to most MSTIDs where the TEC perturbation is both positive and negative. Our observations used the instruments on the CF-3 satellite constellation with the VLA radio telescope to infer characteristics consistent with previous observations of MSTIDs and TWPTIDs. This observation of MSTIDs using an optical sensor on a space-based platform, in addition to another observation of an MSTID from space [*Adachi et al.*, 2011], lays the groundwork for future global studies of MSTIDs using the CF3 satellites and other planned ultraviolet sensors.

[18] **Acknowledgments.** This work was supported in part by the Office of Naval Research. The National Radio Astronomy Observatory (NRAO) is a facility of the National Science Foundation operated under cooperative agreement by Associated Universities, Inc. The VLA observations were funded under NRAO proposal AM-909. We thank the NRAO

staff at the VLA and the CF3 satellite operators in Taiwan for their assistance during the campaign. The GOX and TIP data used in this study were provided by the University Corporation for Atmospheric Research and the National Space Office (NSPO) of the Republic of China (Taiwan).

References

Adachi, T., Y. Otsuka, M. Yamaoka, M. Yamamoto, K. Shiokawa, A. B. Chen, and R.-R. Hsu (2011), First satellite-imaging observation of medium-scale traveling ionospheric disturbances by FORMOSAT-2/ISUAL, *Geophys. Res. Lett.*, *38*, L04101, doi:10.1029/2010GL046268.

Afraimovich, E. L., N. P. Perevalova, and S. V. Voyeikov (2003), Traveling wave packets of total electron content disturbances as deduced from global GPS network data, *J. Atmos. Sol. Terr. Phys.*, *65*(11), 1245–1262.

Anthes, R. A., et al. (2008), The COSMIC/FORMOSAT-3 mission: Early results, *Bull. Am. Meteor. Soc.*, *89*(3), 313–333, doi:10.1175/BAMS-89-3-313.

Bevington, P. R. (1969), *Data Reduction and Error Analysis for the Physical Sciences*, McGraw-Hill, New York.

Budzien, S. A., K. F. Dymond, C. Coker, D. H. Chua, and J.-Y. Liu (2009), Tiny Ionospheric Photometer experiment aboard FORMOSAT-3/COSMIC, *Proc. SPIE*, *7438*, 743813, doi:10.1117/12.826532.

Dymond, K. F., and R. J. Thomas (2001), A technique for using measured ionospheric density gradients and GPS occultations for inferring the nighttime ionospheric electron density, *Radio Sci.*, *36*(5), 1141–1148, doi:10.1029/2000RS002430.

Dymond, K. F., J. B. Nee, and R. J. Thomas (2000), The Tiny Ionospheric Photometer: An instrument for measuring ionospheric gradients for the COSMIC constellation, in *Applications of Constellation Observing System for Meteorology, Ionosphere, and Climate*, pp. 273–290, Springer, New York.

Dymond, K. F., et al. (2008) The Combined Radio Interferometry and COSMIC Experiment in Tomography (CRICKET) campaign, *Proceedings of the 12th International Ionospheric Effects Symposium* (*IES2008*), pp. 621–628, JMG Assoc., Alexandria, Va.

Dymond, K. F., S. A. Budzien, C. Coker, D. H. Chua, and J.-Y. Liu (2009a), Tomographic reconstruction of the low-latitude nighttime electron density using FORMOSAT-3/COSMIC radio occultation and UV photometer data, *Terr. Atmos. Ocean. Sci.*, *20*(1), 215–226, doi:10.3319/TAO.2008.01.15.01(F3C).

Dymond, K. F., S. A. Budzien, C. Coker, and D. H. Chua (2009b), On-orbit calibration of the Tiny Ionospheric Photometer on the COSMIC/FORMOSAT-3 satellites, *Proc. SPIE*, *7438*, 743814, doi:10.1117/12.825316.

Francis, S. H. (1975), Global propagation of atmospheric gravity waves: A review, *J. Atmos. Terr. Phys.*, *37*, 1011–1054, doi:10.1016/0021-9169(75)90012-4.

Hickey, M. P., G. Schubert, and R. L. Walterscheid (2010), Atmospheric airglow fluctuations due to a tsunami-driven gravity wave disturbance, *J. Geophys. Res.*, *115*, A06308, doi:10.1029/2009JA014977.

Hocke, K., and K. Schlegel (1996), A review of atmospheric gravity waves and travelling ionospheric disturbances: 1982–1995, *Ann. Geophys.*, *14*, 917–940.

Jacobson, A. R., and W. C. Erickson (1992a), A method for characterizing transient ionospheric disturbances using a large radiotelescope array, *Astron. Astrophys.*, *257*, 401–409.

Jacobson, A. R., and W. C. Erickson (1992b), Wavenumber-resolved observations of ionospheric waves using the Very Large Array radio telescope, *Planet. Space Sci.*, *40*, 447–455, doi:10.1016/0032-0633(92)90163-I.

Jacobson, A. R., and W. C. Erickson (1993), Observations of electron density irregularities in the plasmasphere using the VLA radio interferometer, *Ann. Geophys.*, *11*, 869–888.

Jacobson, A. R., R. C. Carlos, R. S. Massey, and G. Wu (1995), Observations of traveling ionospheric disturbances with a satellite-beacon radio interferometer: Seasonal and local time behavior, *J. Geophys. Res.*, *100*, 1653–1665, doi:10.1029/94JA02663.

Kassim, N. E., T. J. W. Lazio, W. C. Erickson, R. A. Perley, W. D. Cotton, E. W. Greisen, A. S. Cohen, B. Hicks, H. R. Schmitt, and D. Katz (2007), The 74 Mhz system on the Very Large Array, *Astrophys. J. Suppl. Ser.*, *172*, 686–719, doi:10.1086/518934.

Kotake, N., Y. Otsuka, T. Ogawa, T. Tsugawa, and A. Saito (2007), Statistical study of medium-scale traveling ionospheric disturbances observed with the GPS networks in southern California, *Earth Planets Space*, *59*, 95–102.

Meléndez-Alvira, D. J., R. R. Meier, J. M. Picone, P. D. Feldman, and B. M. McLaughlin (1999), Analysis of the oxygen nightglow measured by the Hopkins Ultraviolet Telescope: Implications for ionospheric partial radiative recombination rate coefficients, *J. Geophys. Res.*, *104*, 14,901–14,913, doi:10.1029/1999JA900136.

Mercier, C. (1986), Observations of atmospheric gravity waves by radiointerferometry, *J. Atmos. Terr. Phys.*, *48*, 605–624, doi:10.1016/0021-9169(86)90010-3.

Picone, J. M., A. E. Hedin, D. P. Drob, and A. C. Aikin (2002), NRLMSISE-00 empirical model of the atmosphere: Statistical comparisons and scientific issues, *J. Geophys. Res.*, *107*(A12), 1468, doi:10.1029/2002JA009430.

Schunk, R. W., and A. F. Nagy (2000), *Ionospheres: Physics, Plasma Physics, and Chemistry*, pp. 274–275, Cambridge Univ. Press, New York.

Tinsley, B. A., and J. A. Bittencourt (1975), Determination of F region height and peak electron density at night using airglow emissions from atomic oxygen, *J. Geophys. Res.*, *80*, 2333–2337, doi:10.1029/JA080i016p02333.

Titheridge, J. E. (1971), Nonperiodic irregularities in the ionosphere, *J. Geophys. Res.*, *76*, 6955–6960, doi:10.1029/JA076i028p06955.

Tsugawa, T., Y. Otsuka, A. J. Coster, and A. Saito (2007), Medium-scale traveling ionospheric disturbances detected with dense and wide TEC maps over North America, *Geophys. Res. Lett.*, *34*, L22101, doi:10.1029/2007GL031663.

Watts, C., K. F. Dymond, C. Coker et al. (2008), A medium-scale traveling ionospheric disturbance observed from the ground and from space, *Eos Trans. AGU*, *89*(53), Fall Meet. Suppl., Abstract SA33A-1623.

P. A. Bernhardt, Plasma Physics Division, Naval Research Laboratory, Washington, DC 20375, USA.

S. A. Budzien, C. Coker, K. F. Dymond, and P. S. Ray, Space Science Division, Naval Research Laboratory, Washington, DC 20375, USA. (kenneth.dymond@nrl.navy.mil)

T. Clarke, N. Kassim, and K. Weiler, Remote Sensing Division, Naval Research Laboratory, Washington, DC 20375, USA.

S. Close, Department of Aeronautics and Astronautics, Stanford University, Durand Bldg., 496 Lomita Mall, Stanford, CA 94305-4035, USA.

A. Cohen, Applied Physics Laboratory, Johns Hopkins University, 11100 Johns Hopkins Rd., Laurel MD 20723-6099, USA.

P. Colestock, Los Alamos National Laboratory, PO Box 1663, Los Alamos, NM 87545, USA.

P. C. Crane, 1206 Lewis Dr., Socorro, NM 87801, USA.

A. Datta, Center for Astrophysics and Space Astronomy, University of Colorado, 389 UCB, Boulder, CO 80309-0389, USA.

M. Kuniyoshi and F. Schinzel, Max-Planck-Institut für Radioastronomie, Auf dem Hügel 69, D-53121 Bonn, Germany.

T. J. Lazio, Jet Propulsion Laboratory, M/S 138-308, 4800 Oak Grove Dr., Pasadena, CA 91109, USA.

S. Myers, National Radio Astronomy Observatory, Array Operations Center, PO Box O, 1003 Lopezville Rd., Socorro, NM 87801–0387, USA.

Y. Pihlstrom, L. J. Rickard, and G. B. Taylor, Department of Physics and Astronomy, University of New Mexico, 1919 Lomas Blvd. NE, Albuquerque, NM 87131, USA.

C. Watts, Diagnostics Division, ITER, Route de Vinon sur Verdon, F-13115 St Paul Lez Durance, France.